



**FACULTY OF SCIENCE AND TECHNOLOGY**

## **MASTER THESIS**


Study programme / specialisation:

Masters in Industrial Asset Management

Author: Anmol Bhattarai

Spring semester, 2022

Open / ~~Confidential~~



(signature)

Supervisor  
Wiktor Weibull

Thesis title:  
Seismic Assessment of Offshore Monopile Foundation  
With Variable Magnitude Moments

Credits (ECTS): 30

Keywords: Finite element, Monopile,  
Seismic, ABAQUS, Limit State

Pages: 35

+ appendix: 4

Stavanger, 06/14/2022  
date/year

# Declaration of Authorship

I, Anmol Bhattarai, declare that this thesis titled, Seismic Assessement of Offshore Monopile Foundation with variable magnitude moments and the work presented in it are my own. I confirm that:

- This work was done wholly or mainly while in candidature for a master's degree at this University.
- Where I have consulted the published work of others, this is always clearly attributed.
- Where I have quoted from the work of others, the source is always given. With the exception of such quotations, this thesis is entirely my own work.
- I have acknowledged all main sources of help.

Signed: 

Date: 15.06.2022



# *Abstract*

The recent advances in offshore technology has led to deeper exploratory excursions, easier structure installation and monitoring as well as remotely-monitored maintenance work , which has been a primer for increase in offshore structures worldwide. Ensuring the structural integrity is the foreground for any design or maintenance operation. Monopile support structures are one of the mostly used and important structural component for the general stability and longevity of OWT installed at lower level of water depth. A finite element analysis method is used to model and analyse the limit states of a monopile in a sand-clay multi-layer soil model with environmental loads along ranging magnitude of earthquake. The stress generated, pile deflection and pile rotation on the monopile is studied and compared to the ultimate limit state of the monopile, over which it would go into failure. The results show that the monopile movement w.r.to horizontal deflection and rotation exceed the recommended limit states at higher magnitudes of earthquake. This showcases, the need of seismic analysis and regulatory assessment of monopile foundation in seismically active areas.

# *Acknowledgements*

The completion of this thesis work was possible due to cumulative help of many. I would like to thank the UiS faculty for materials and materials science for all the technical resources provided for the thesis work. I would like to thank my supervisor Mr. Wiktor Weibull for help and recommendations he provided for the success of this work. Lastly I would like to thank my families and friends who supported and motivated me for the entire duration of thesis work.

# Contents

Declaration of Authorship	i
Abstract	iii
Acknowledgements	iv
Abbreviations	vii
<b>1 Introduction</b>	<b>1</b>
1.1 Motivation . . . . .	1
1.2 Objectives and Scope of Work . . . . .	2
1.3 Relevant works . . . . .	2
1.4 Challenges . . . . .	3
<b>2 Theoretical Framework</b>	<b>4</b>
2.1 Support structures for offshore wind turbine . . . . .	4
2.2 Monopile foundation . . . . .	5
2.3 Soil Model . . . . .	6
2.3.1 Soil Properties . . . . .	7
2.3.2 Mohr Coulumb Model . . . . .	8
2.3.3 Liquefaction in Soil . . . . .	8
2.4 Load selection for Monopile foundation . . . . .	9
2.5 Seismic waves . . . . .	9
2.5.1 Types of faults . . . . .	10
2.5.2 Seismic waves propagation . . . . .	11
2.5.3 Seismic Properties . . . . .	12
2.5.4 Use of ground motion prediction equations . . . . .	13
2.6 Limit State of a system . . . . .	15
<b>3 Solution Approach</b>	<b>17</b>
3.1 Creating a Finite element model . . . . .	17

3.1.1	Monopile structure . . . . .	18
3.1.2	Soil Properties . . . . .	18
3.1.3	Mesh quality . . . . .	20
3.1.4	Boundary condition and pre-defined fields . . . . .	20
3.1.5	Soil Structure Interaction . . . . .	22
3.1.6	Step-definition . . . . .	23
3.2	Loads used for the modelling process . . . . .	23
3.2.1	Induced loads . . . . .	24
3.2.2	Environmental loads . . . . .	25
3.3	Test Models . . . . .	26
<b>4</b>	<b>Results and Analysis</b>	<b>28</b>
4.1	Experimental results . . . . .	28
4.1.1	Case 1 . . . . .	28
4.1.2	Case 2 . . . . .	29
4.1.3	Case 3 . . . . .	31
4.1.4	Case 4 . . . . .	32
4.2	Analysis . . . . .	33
<b>5</b>	<b>Conclusion and Recommendations</b>	<b>35</b>
	<b>List of Figures</b>	<b>35</b>
	<b>List of Tables</b>	<b>37</b>
<b>A</b>	<b>Appendix</b>	<b>38</b>
A.1	PSA vs Time graph for all Moment magnitudes . . . . .	38
A.2	Rotation at pile node . . . . .	41
	<b>Bibliography</b>	<b>43</b>

# Abbreviations

Acronym	What (it) Stands For
FEM	Finite Element Method
NREL	National Renewable Energy Laboratory
NGA	National Geospatial-Intelligence Agency
OWT	Offshore Wind Turbine
GMPE	Ground Motion Prediction Equations
PSA	Pseudo Spectral Acceleration
PEER	Peer's Enriching Each others' Recovery
API	American Petroleum Institute
ULS	Ultimate Limit State
IOT	Internet of Things



# Chapter 1

## Introduction

### 1.1 Motivation

The offshore industry scope has been well adjusted to the new changes taking place over the years. There have been a lot of changes in the applicability of different analytical methods to make sure the assets have sufficient structural integrity and behaviour for higher operational time and reduced down times. Assets in offshore industries have also grown more compact with the use of complex systems, with different sub-systems working through integrated operations using IOT and sensors. Improvement in asset management concepts has also led to more emphasis in asset monitoring, material behaviour and maintaining Health and Safety Protocols.

With emphasis on green and sustainable energy sources, wind power has been a major focus of research and innovation by governmental agencies, energy companies and scholars. With advances in offshore technology, offshore structures have been widely utilized in the recent years which has led to development of operations, maintenance and design operations. Ensuring the structural integrity is the foreground for any design or maintenance operation. Substantial studies have been done in order to inspect the structural integrity of the OWT foundations primarily in frequency domain for modal analysis of resonance behaviour in the structure. Less studies have been done in analysis methods focusing on the soil-structure interaction and the effects of environmental loadings. This thesis work will primarily focus on environmental, especially seismic loads acting on the structure and their effects. Though the historical observations of significant structural damage in a turbine foundation during earthquakes has been low, the total risk, when we

consider a "wind farm" , with numerous wind turbines, especially from an economic consideration can be quite substantial [14].

## 1.2 Objectives and Scope of Work

Offshore foundations are subjected to complex loading conditions, resultant of both the operational and environmental conditions, which requires a complex modelling as well as analysis procedure to understand the potential failure conditions that can occur. The aim of this master thesis is to conduct a finite element structural analysis of monopile foundation of offshore wind turbine primarily focused on seismic loading and earthquake effect. Main emphasis is done to examine the deformation occurring in monopile foundation subjected to different loading conditions, and realistic soil model properties. The thesis work is structured in 3 steps. The first step provides, fundamental theoretical background required for modelling and analysis of the soil and structure. This involves theory related to monopile supports, soil modelling and different load parameters relevant to the thesis work. The second step provides modelling techniques and steps taken in order to conduct the analysis. This involves implementation of the input parameters, boundary conditions and case scenarios. The final step provides analysis and results obtained from step 2 and subsequent relation with studies already conducted in similar domains.

## 1.3 Relevant works

Studies conducted in OWTs are relatively less extensive compared to onshore foundations [14]. This is due to the fact that installation of onshore foundations date back to a longer time than offshore turbine. Also, installation of offshore turbines in seismically active zones have been a more recent trend, after the global rise in offshore structures and haven't been a main focus of research. Study in limit states of the monopile foundation under range of PGAs has been done by [7] and shows the vulnerability under extreme earthquakes especially for soft soils need to be addressed and researched more in case of offshore turbines. The research is limited in the soil-structure interaction in the model, as a more simplified p-y model is used. Similarly, experimental research has been done by [4] to study the effects of concurrent environmental loads (wind, wave and current loads) on monopile turbines.

The vulnerability of offshore foundation under seismic loading , especially under consideration of non-linear soil characteristics and pore pressure accumulation has been demonstrated through soil settlement and consequent permanent deflection in case of monopile foundation[15] .

## **1.4 Challenges**

A 3-D FEM modelling approach requires inputs for basic structural parameters, material parameters, load types and conditions ,interaction parameters and adequate meshing technique. Accuracy and complexity of finite element based analytic simulations, depends highly on the variables included on the simulations. To streamline the simulation time and workload, some deliberate considerations have been made on the model. Experimental input parameters are taken from relevant literature, and synthetic data are taken typically from recognised databases/ repository. Some parameters are also estimated, where previous works do not provide relevant information. This has led to a more general structural assesement instead of a real-case scenario.

# Chapter 2

## Theoretical Framework

### 2.1 Support structures for offshore wind turbine

The recent advances in offshore technology has led to deeper exploratory excursions, easier structure installation and monitoring as well as remotely-monitored maintenance work , which has been a primer for increase in offshore structures worldwide. Global cumulative installed capacity for offshore wind has seen an increase from 24000 to 32905 MW from the year 2018 to 2020 [17]. Structural integrity and resistance against environmental loadings are heavily dependent upon the foundation shape and type. In fact, one-third of the overall turbine cost is contributed to foundation installation and design. Selection of turbine foundation structures, especially for offshore is of huge importance, as the general stability, and longevity of the whole structure depends upon the dynamic load that the support can hold. The primary criteria for selection of structure foundation is dependent upon the deformation tolerance, i.e. maximum limit of rotation of the pile head/ pile head tilt. [16] Base structures for OWT are selected primarily based on the turbine ratings(rated capacity), depth of the seabed and the distance from shore. Mostly used offshore turbine foundation includes gravity foundation, monopile foundation, floating tension leg, jacket foundation . The applicability and use of these structures based on the criterions are tabulated as in table 2.1 .

**Table 2.1:** Foundation and Water depth

Type of structure	Recommended water depth
Gravity	$\leq 10\text{m}$
Monopile	15-40m
Tripod foundation	10-35m
Jacket foundation	5-50m
Floating structure	$> 60\text{m}$

## 2.2 Monopile foundation

Monopiles are one of the mostly used foundation types on offshore with water depth in between ( 15 -40m ) range. Monopile construction consists of a hollow cylindrical structure of varying dimension, and is embedded into the sea bed to certain depth. Monopiles are widely used due to their ease of installation, repairability/modification and are structurally simple. Monopile foundations consist of a single steel pile driven into the soil. The foundation is connected to the turbine structure tower using a steel transition piece. Transition piece also acts as an access point for maintenance work and cable connections. For simplicity of modelling, similar material properties and significantly lower impact of transitional piece in structural analysis, the monopile foundation is modelled without the transitional piece and the length of the transitional piece is considered in the cylinder pile itself. Fig 2.1 illustrates the monopile model used for the analysis as well as a typical representation of wind turbine model with transition piece intact.

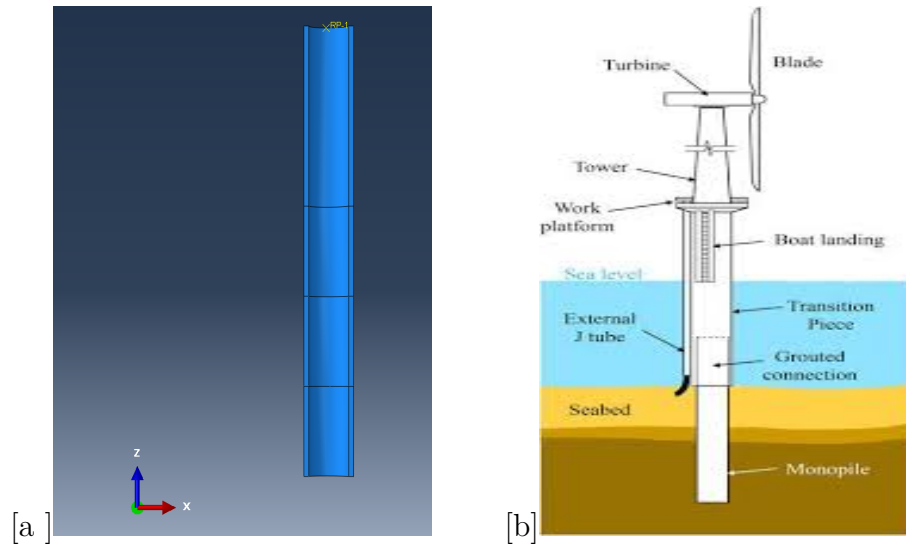


**Figure 2.1:** FEM Monopile model and monopile model with a transition piece [18]

## 2.3 Soil Model

Soil is a product of chemical and physical weathering of rock into smaller particles. It consists of particles of organic matters, minerals, clay, silt or sand and also combination of all of these. As, soil is formed by a natural process of disintegration of rocks, the corresponding properties of each soil is inherently different.

This makes soil modelling a complex process. Variation in material behaviour of soil depending upon the loading and unloading conditions, adds more to the complexity of modelling. Also, soil composition and its properties change substantially with increase in soil depth. There have been many techniques used for soil modelling. Numerical models based on P-Y( Soil resistance/deflection) curves have been used for analysis where, the soil behaviour is represented by a series of non-linear springs. This is a relatively simple modelling method with less computational time needed. But, the soil mechanisms reflected by p-y curves are deemed unsatisfactory especially for monopile foundations on offshore due to their lower (L/D) ratio [1]. A continuum modelling of soil with solid elements is a more complex procedure with the use of finite element analysis and uses more computational time as well as need of more material parameters. But it provides easier switching/combination of soil types, and also provides easier modelling of soil interaction w.r.to any structure. In our methodology, the soil layers are provided with differing material properties

w.r.to the depth and failure criterion and response to shear and normal stress are modelled using Mohr Coulumb model .

### 2.3.1 Soil Properties

Due to non-linear properties, soil modelling is different from other material modelling (e.g. steel, concrete) with linear properties. Some significant material parameters are defined, which are relevant to the scope of this thesis work.

#### Porosity

A soil layer may consist of 3 primary elements i.e. solid particles, liquid and gas [9]. Presence of non-solid particles lead to porous structure in the soil. The porosity in our thesis work is defined through void ratio ( $e$ ) i.e.

$$e = V_p/V_s \quad (2.1)$$

where  $V_p$  is the volume of pores and  $V_s$  is the volume of solids.

Presence of air or other gases are not included in the scope of this thesis, so saturation properties are of less relevance.

#### Unit Weight of soil

Volumetric or unit weight of soil is defined as :

$$\gamma = \frac{W}{V_t} = \frac{mg}{V_t} = \rho g \quad (2.2)$$

This formula can be further simplified in terms of void ratio, density of water and density of solid particles as:

$$\gamma = \frac{W}{V_t} = S_n \rho_w g + \left(1 - \frac{e}{e+1}\right) \rho_p g \quad (2.3)$$

### 2.3.2 Mohr Coulumb Model

Mohr Coulumb Model is a generalised mathematical model for calculating response in brittle materials( concrete, soil) with shear and normal stress .This model is significant in deriving the inelastic property of soil. It is widely used due to its simplification and need of only a few modal parameters for a realistic assessment of soil failure at different principal stresses. The Mohr Coulumb Criterion is described by four major parameters and is written as:

$$\tau = c + \sigma \tan \phi \quad (2.4)$$

, where  $\tau$ = shear stress,  $\sigma$ = normal stress ,  $c$ = cohesion in the material and  $\phi$ = angle of friction

The maximum allowable shear stress in the soil is defined by the yield line (see fig. 2.2) and is dependent upon the cohesion of the material and the angle of friction. Stress values under the yield line is deemed elastic and vice versa. The cohesion and friction properties is dependent on the soil type, initial soil conditions and the loading conditions. So, their values are not constant.

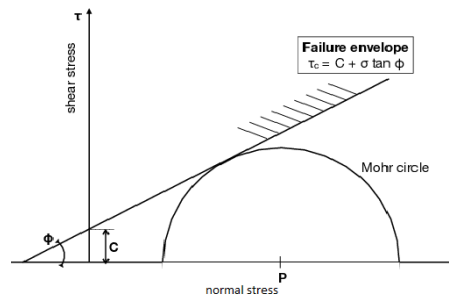


**Figure 2.2:** Mohr-Coulumb failure criteria and Mohr's Circle

### 2.3.3 Liquefaction in Soil

Soils with lower cohesiveness, under instantaneous/sudden stress undergo a phenomenon of liquefaction, during which the soil loses the stiffness and strength. This sudden change leads to the solid soil, acting like a liquid. This phenomenon can be seen as quicksand in popular culture but can occur in both clay and sand.



During seismic loading, soil can undergo similar phenomenon, which can lead to the instability and uneven settlement of structure above the soil layer. In case of loose sand, as used in the model, strain-softening occurs, when the shear stress is greater than the ultimate shear strength of the soil.

## 2.4 Load selection for Monopile foundation

Loads/forces acting on Monopile in offshore environment involves the induced forces by the turbine as well as the environmental forces acting on the structure. Environmental loads acting on the structure are largely dependent upon the climate, topology and geographical region of the installation. In extreme temperature conditions, the ice load effects can be highly significant. Similarly, based on habitat and geographical regions, environmental effects from sea-dwelling organisms, bottom dwelling organisms as well as avian life forms can have a great significance with reference to the ecological and sustainable integrity[10].

In this study, load distribution on Monopile Foundation are classified as induced loads and environmental loads. Seismic loads and hydrodynamic loads are taken into account as environmental load. As, the model incorporates only the parts beneath sea level, wind loads are not considered in this study. Environmental effects from organisms and ice loading are also not included in the scope of this thesis.

## 2.5 Seismic waves

Seismic waves, the precursor of earthquakes are generated from the earth, caused due to geological faults and subsequent movement of the tectonic plates. The low-frequency acoustic energy induced by these seismic waves, when subjected to any structure generate seismic loads on the structure. Based on the intensity of these waves(i.e. frequency content) these loads can range from less significant to catastrophic. In offshore environment, with high seismic activity, seismic loads are of a great importance, and requires consideration during design as well as operations.

### 2.5.1 Types of faults

Faulting results in permanent deformation of rock, acting corresponding to the movement of tectonic plates relative to each other. As, earthquakes are already established to be formed due to geological faults, the types of faults that can occur need to be addressed. Faults always occur across 2 rock blocks, also known as fault blocks. Hanging wall is the fault block above the line where the fault occurs (fault line) and foot wall is the fault block below the region where fault occurs. Different fault types occur due to different interactions between the hanging wall and the foot wall.

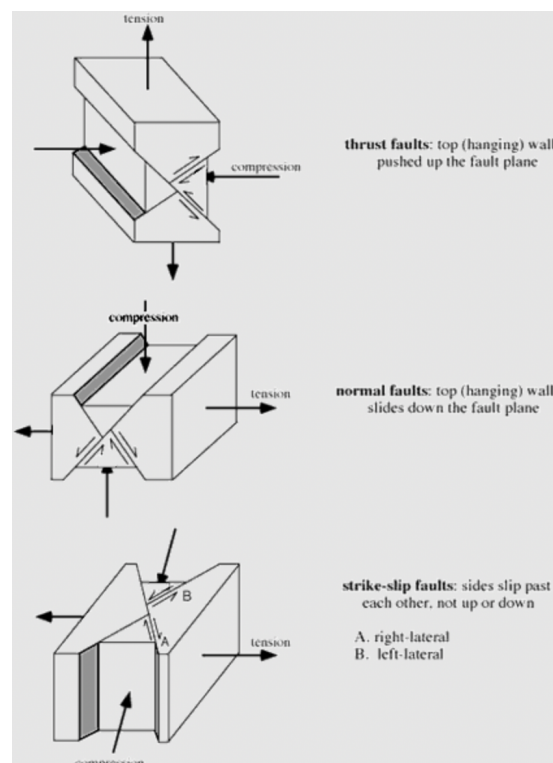


**Figure 2.3:** Major fault types during an earthquake (source:ucmp.berkeley.edu)

#### Strike-Slip Fault

Strike-slip fault occurs when the fault blocks slip past each other parallel to the fault line. This causes a lateral movement of the fault blocks instead of a vertical movement. It is caused by shearing stress

### **Normal Fault**

Normal fault occurs when the hanging wall moves down relative to the foot wall. It is caused by extensional stress in the earth's crust resulting in pulling apart between the 2 fault blocks.

### **Reverse Fault**

Reverse fault occurs when the hanging wall moves up relative to the foot wall. It is caused by compressional stress, acting along the horizontal direction between 2 fault blocks.

## **2.5.2 Seismic waves propagation**

Seismic waves propagate from the earth's crust in the form of stress waves, whenever an earthquake occurs. These waves travel in the form of body waves and surface waves. Body waves travel through the interior of the earth surface and are further classified into P-Waves and S-waves. P-waves are compressive in nature and travel faster in soil medium due to increase in stiffness of soil during compression. S-waves move in direction perpendicular to the particle motion, and hence create shear deformation in the propagating medium. Surface waves travel in form of Rayleigh and Love waves and are generated due to the interaction of the body waves with the surface of the ground. Surface wave acting similar to Rayleigh wave, is Scholte wave, which propagates between liquid and solid medium, and is the major inducing wave for ground shaking in seabed. Wave propagation characteristics of the seismic waves are shown in fig. [2.4\[3\]](#).

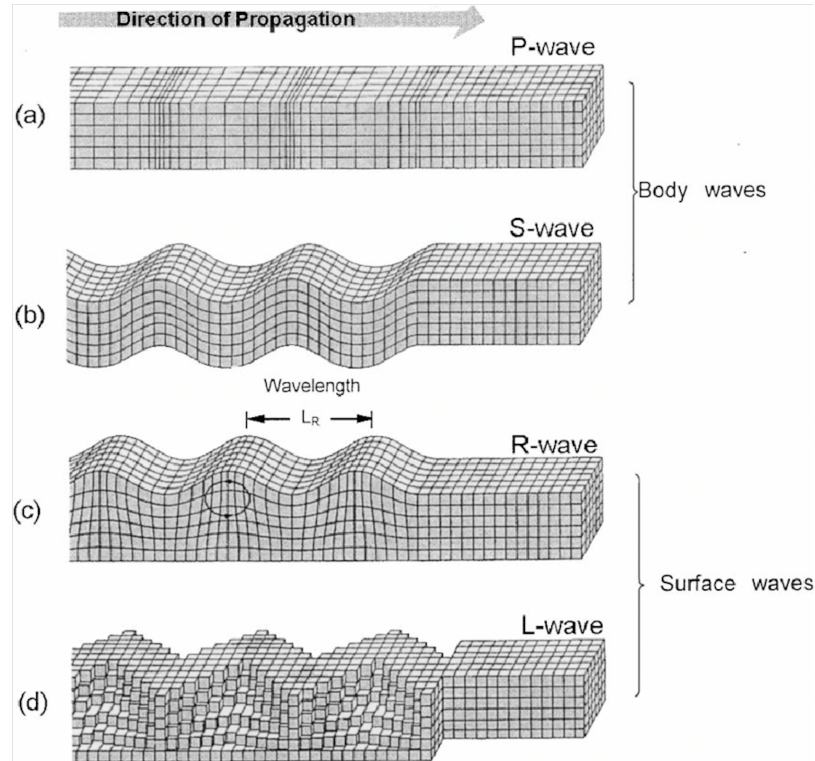


**Figure 2.4:** Wave propagation of seismic waves

### 2.5.3 Seismic Properties

From structural point of view, surface waves have higher amplitude and they travel on the the surface layer of the earth and can cause more damage to the structures on surface . The elliptical movement of Scholte Waves, normal to the surface have greater impact on the turning moments and displacement of the structures. Especially, the horizontal component of these waves have greater impact on the structural integrity of a structure. Seismic loads are considered in the horizontal directions only in the analysis method.

#### Shear Modulus and shear Velocity

The shear modulus of the waves propagating in perpendicular direction is dependent upon the motion of the particle and the density of the medium, and is given as:

$$G = \frac{E}{2(1 + \nu)} \quad (2.5)$$

And we calculate the shear wave velocity as:

$$V_s = \sqrt{\frac{G}{\rho}} \quad (2.6)$$

From the point of seismic hazard analysis, the averaged shear wave velocity, within a certain depth provides accurate assessment for near surface structures. Averaged shear velocity within 30m depth is adapted for the thesis work. And is given by:

$$V_s^{30} = \frac{30}{\sum_{i=1}^N (d_i/v_i)} \quad (2.7)$$

where,  $d_i$  and  $v_i$  are the depth and shear velocity of N layers within 30m depth.

### **Moment Magnitude**

Moment magnitude is a scale used for measuring the strength of an earthquake. The moment magnitude of a particular earthquake is derived from the amplitude spectrum of the earthquake and is scaled according to the similar moment generated on other earthquakes with the largest energy release.

### **Damping**

Damping is the loss of energy during a periodic cycle of loading. As, the soil layers under seismic loads undergo energy dissipation in subsequent cycles of loadings, damping parameter is needed to be addressed. Damping in the seismic assessment is defined through damping ratio, which is a ratio of actual damping in the system and critical damping in the system (min. value of damping required to return the particles to initial state of zero amplitude in the fastest time.)

$$\zeta = \frac{C_0}{C_c} \quad (2.8)$$

#### **2.5.4 Use of ground motion prediction equations**

Ground Motion Prediction Equations (GMPE) are used for motion prediction on a given area in regards to the motion's acceleration, velocity or displacement. GMPE

uses a finite number of input parameters to predict the motion characteristics, as all the parameters for an accurate prediction of ground motion is associated with a lot of uncertainties and variables which are site specific and not always recorded or available. GMPE provides a fair estimation for conducting seismic analysis and risk assessment of structures.

### Source and distance parameters

Some major input parameters and estimations required for GMPE calculations are illustrated in brief and include several source, path and site parameters. Estimation of some parameters are derived from [13]. Illustrations of these parameters are shown in fig. 2.5.

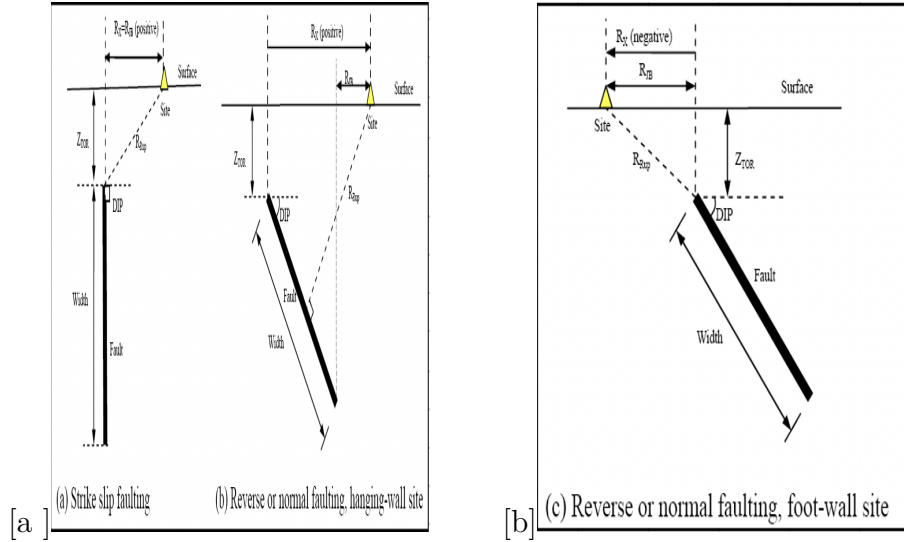


**Figure 2.5:** Illustrations of GMPE parameters (source: NGAW2 database)

Fault dip angle  $\delta$  : It is the angle made by the fault w.r.to the horizontal. Dip angle can be assumed  $90^\circ$  for strike slip fault. And recommended average values for normal and reverse fault are  $50^\circ$  and  $40^\circ$  respectively.

Focal depth of earthquake  $Z_{HYP}$  : Hypocentral depth/ Focal depth is the distance from the surface to the region where earthquake forms. It can be estimated , based on the fault type and moment magnitude as:

$$Z_{HYP} = \begin{cases} 5.63 + 0.68M & \text{for strike-slip faulting} \\ 11.24 - 0.2M & \text{for non-strike-slip faulting} \\ 7.08 + 0.61M & \text{for general (unspecified) faulting} \end{cases} \quad (2.9)$$

Rupture width (W) : It is the average width of the rupture surface. Rupture width is calculated ,always in the downdip direction. Rupture width is also estimated, depending upon the fault type and moment magnitude as :

$$W = \begin{cases} 10^{-0.76+0.27M} & \text{for strike-slip events} \\ 10^{-1.61+0.41M} & \text{for reverse events} \\ 10^{-1.14+0.35M} & \text{for normal events.} \end{cases} \quad (2.10)$$

Joyner-Boore distance  $R_{JB}$ : It is the horizontal distance from the site to the surface projection of the rupture.  $R_{JB}$  can be approximated to the source-to site distance for easier calculations/approximation.

Site coordinate  $R_X$ : Horizontal distance to the top edge of the of rupture measured perpendicular to the strike , is a necessary path parameter used in calculations. It is calculated as

$$R_X = R_{JB} \sin \alpha$$

where,  $\alpha$  is the source to site azimuth, estimated as  $50^\circ$  for hanging wall site and  $-50^\circ$  for foot wall site, as per average values in NGA files.

Rupture Distance  $R_{RUP}$  : It is defined as the closest distance of the site to the rupture plane. It is calculated as:

$$R_{RUP} = \sqrt{(R_{RUP})^2 + |R_X \cot \alpha|^2}, \text{ where}$$

$$R'_{RUP} = \begin{cases} \sqrt{R_X^2 + Z_{TOR}^2} & \text{for } R_X < Z_{TOR} \tan \delta \\ R_X \sin \delta + Z_{TOR} \cos \delta & \text{for } Z_{TOR} \tan \delta \leq R_X \leq Z_{TOR} \tan \delta + W \sec \delta \\ \sqrt{(R_X - W \cos \delta)^2 + (Z_{TOR} + W \sin \delta)^2} & \text{for } R_X > Z_{TOR} \tan \delta + W \sec \delta \end{cases} \quad (2.12)$$

## 2.6 Limit State of a system

For any system, a threshold up to which the system can function for a given state, needs to be addressed in order to define the failure point of the system.

For structural components, capable of breaking, buckling or bending, limit of the structure up to which it can withstand failure is defined through its limit state. In case of monopile, dynamic lateral and vertical loads act simultaneously at varying points of the structure. Usually these limit states are defined as engineering demand parameters in terms of stress, displacement, bending and rotation. When an operational limit state of a system (i.e. limit up to which the system can successfully operate, also known as Serviceability Limit State) is to be calculated, modal parameters, operating range and operating loads are considered, surpassing which, the system fails to operate.

**Table 2.2:** Stability criterias

Limit parameter	Limit Value
Pile yield	Yield strength of 355 MPa
Allowed deflection at mudline	0.2 m
Allowed rotation at mudline	0.5°

Ultimate Limit State of a structure is the maximum limit after which the structure collapses or undergoes permanent deformations. Limits during abnormal loading cases, or harsh environmental conditions are typically addressed through Ultimate Limit State, when serviceability of the system is not of the main concern. The design criteria for monopile foundation stability must adhere to fundamental criteria of maximum allowable rotation at mudline and maximum deflection at pile toe [20]. As, the thesis work predominantly focuses in lateral forces, the lateral deflection and rotation values are considered. Due to a lack of precise values of these allowable limits, case values from [2] and presented in table 2.2.



# Chapter 3

## Solution Approach

### 3.1 Creating a Finite element model

Numerical approaches for seismic analysis has been done numerous times based on classical linear static analysis, by calculating the seismic loading through analyzing response spectrum in a single degree of freedom system. Main drawback of this approach has been the lack of accounting for load distribution and non-linearities developed in the system or simplified structure [6] . A nonlinear dynamic analysis based on the time history for a detailed physical structure using corresponding material, contact properties and loading conditions is more effective for a structural analysis, and has been the approach used in this thesis. All modelling is done through Finite Element Software, ABAQUS because of its global acceptance in scholar literature, ease of access and ease of modification. Also, due to symmetry of the soil-monopile structure, the modelling is done only for the half profile with symmetry along the Y-axis. This helps with the overall computing time for the simulation run.

Finite element modelling process requires several input requirement for definition of the model, interaction between the model substructures and environmental conditions. It also includes the definition of the output parameters that is aimed to get from the simulation. The input file is fed into the processing unit of the modelling software and results are obtained as simulated plots, animations as well as requested output data values at specific points in the model. A process flow diagram for the working of the ABAQUS interface is shown in fig. 3.1.

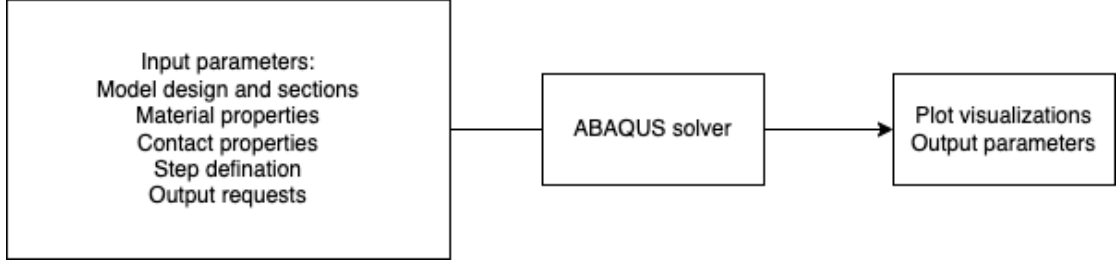


**Figure 3.1:** Process diagram for ABAQUS simulation

### 3.1.1 Monopile structure

Modelling of the monopile structure is done as a uniform cylindrical hollow tube with a thickness of 6cm, diameter of 6m and overall length of 30m. The design considerations are made fulfilling the API code[12] requirement of minimum thickness

$$t[mm] \geq 6.35[mm] + \frac{D[mm]}{100} \quad (3.1)$$

and D/t ratio of <120. The structure is considered as half embedded in the sea bed and half of it is exposed to the sea water, and considered as an isotropic elastic material. Selection of material is done as S355 steel for the whole structure with Youngs Modulus=2.1e+5 MPa,  $\nu=0.3$  and density=7850  $kg/m^3$ .

### 3.1.2 Soil Properties

Soil surface interacting with the monopile is modelled as a rectangular soil-pile with a length of 60m, breadth of 45m and an overall height of 30m. The soil structure is layered into 4 different layers with differing soil properties of mass density, cohesiveness, angle of friction as shown in table 3.1. Layering of the soil layer is done to provide a more realistic approach towards soil pile interaction. The volume of soil model is taken considerably larger than the monopile volume in order to eliminate any boundary effects that can occur in the whole model[21].

Mohr-Coulomb method is a typically used model for soil and concrete modelling. In this model, we consider the soil material as elasto-perfectly plastic. The clay layer property is derived from London Clay and properties of sandy layer from different sources. Soil properties based on Mohr-Coulomb Model for both soil types is taken with respective properties given in table 3.2.

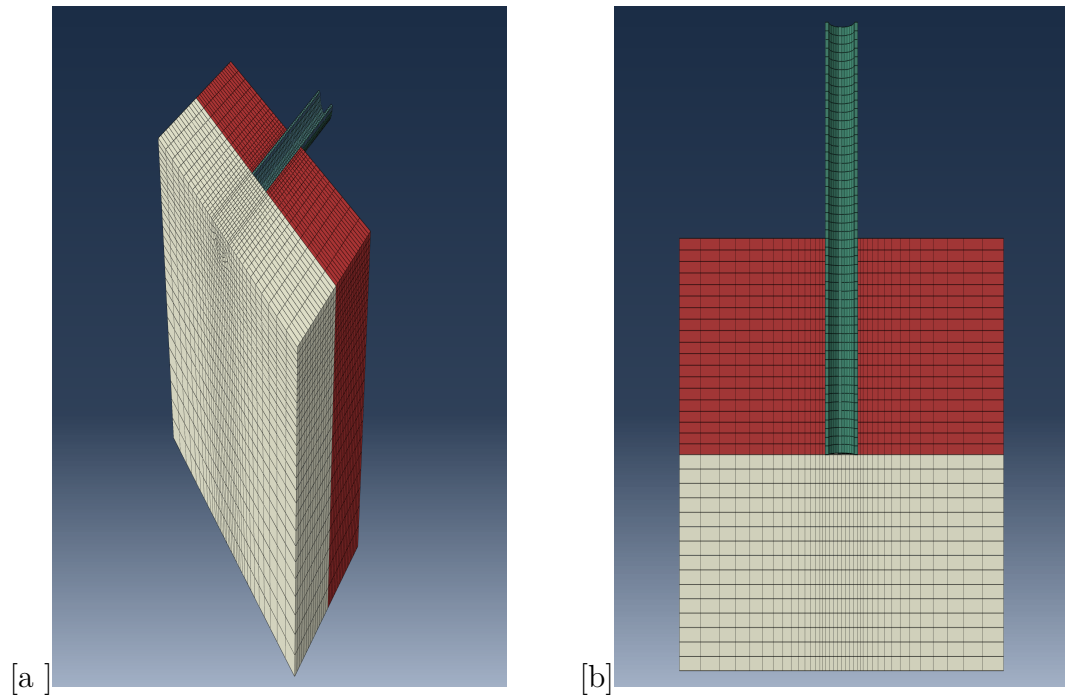
**Table 3.1:** Soil layer and their corresponding properties

Soil layer	Soil type	Mass density(kg/m <sup>3</sup> )	Young's Modulus (MPa)
Layer 1	sand	1430	12
Layer 2	sand	1435	12
Layer 3	sand	1440	12
Layer 4	sand	1430	12
Layer 5	clay	1330	50

**Table 3.2:** Mohr-Coulomb Model properties

Parameters	Sand	Clay
Friction angle	36 °	20
Dilation angle	6 °	0
Cohesive Yield Stress	300 $N/m^2$	13500 $N/m^2$
Abs. Plastic Strain	0	0
Void ratio	0.5	2

Finite element analysis for soil layer is done with standard, linear, pore fluid/stress linear Hex element . Model of the whole structure with corresponding layers of soil is shown in fig. 3.2.

**Figure 3.2:** Front and isometric view of different soil layers

### 3.1.3 Mesh quality

To help with contact and convergence problems, the mesh size of soil model is set as "coarse" and mesh size of the monopile is taken as finer. The global size of elements in the monopile is taken as 0.8. For the soil model, the element size is taken from 2 to 0.8, with biasing towards the center. Both meshes are then verified for poor-elements, and discontinuities in the mesh. Elements and nodes in each structure is highlighted in table 3.3.

**Table 3.3:** Elements and Nodes in the model

Instance	Elements	Nodes	Element type
Soil foundation	34502	37905	C3D8RP
Monopile	700	1530	C3D8R

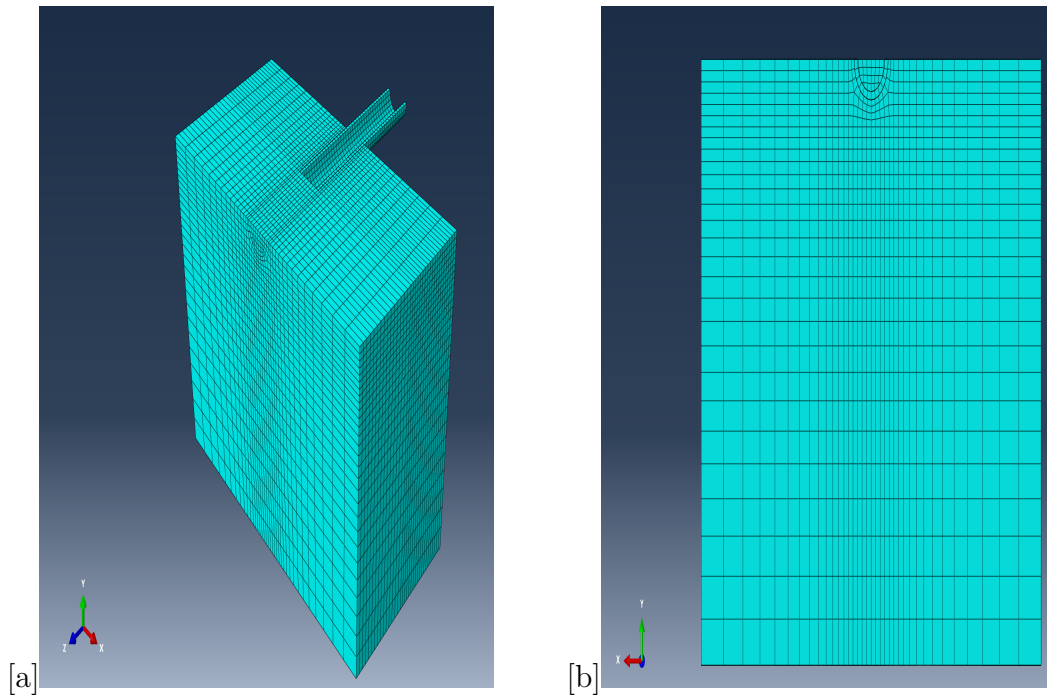


**Figure 3.3:** Meshed Structure of soil-monopile assembly

### 3.1.4 Boundary condition and pre-defined fields

Displacement of the Bottom layer of the soil structure is constricted in all coordinates ( $U_1, U_2$  and  $U_3$ ) during the geostatic and static load steps and then only in the Y and Z directions during seismic loading, for seismic acceleration in the

X-direction. Particles at the boundary are confined in x-direction displacement. The 2 boundary conditions are shown in fig. 3.4.

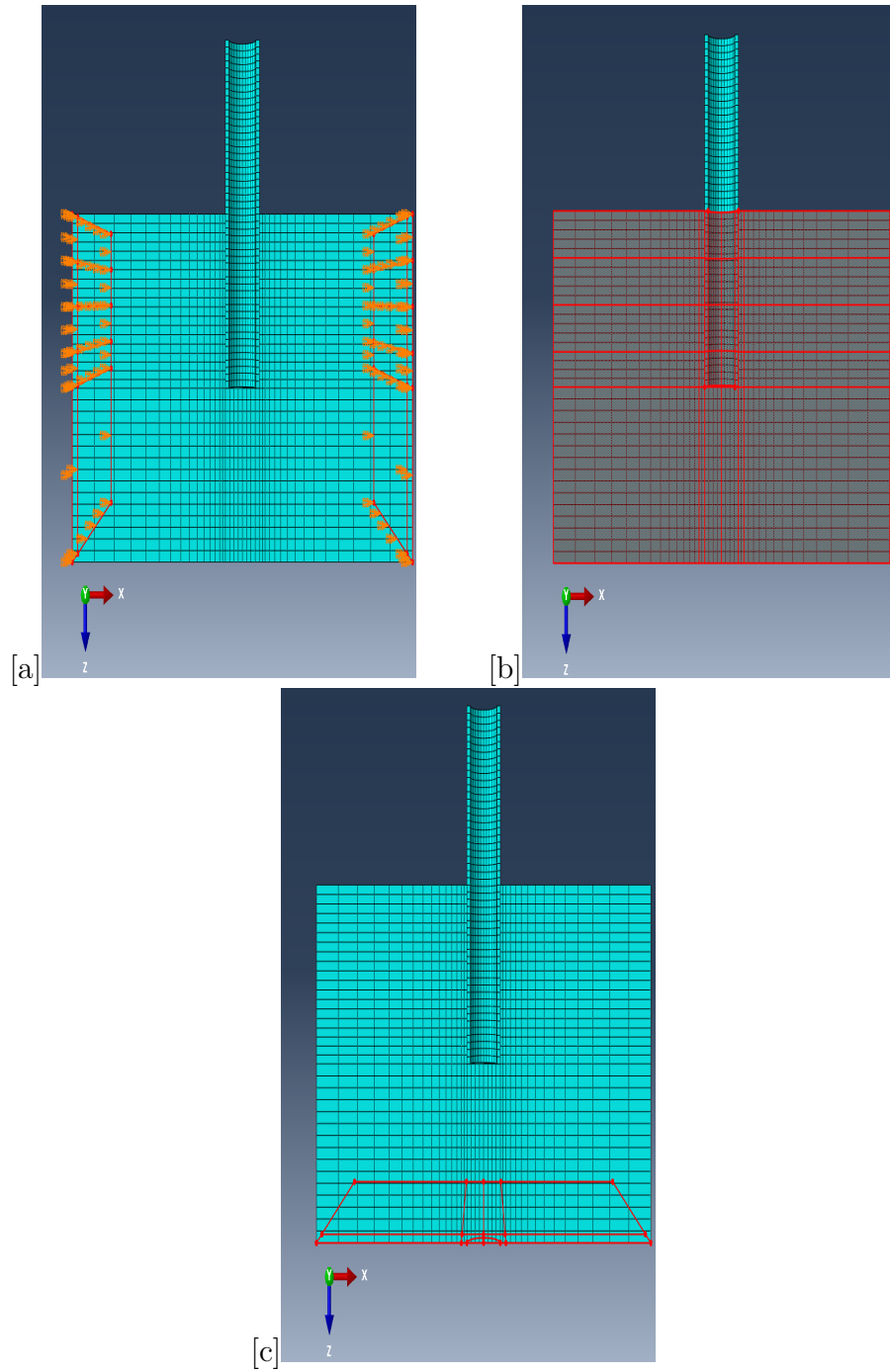


**Figure 3.4:** Boundary conditions applied on the model

### 3.1.5 Soil Structure Interaction

Non-linearity between the monopile and soil model is modelled through contact pairs. Monopile and soil structure form contact pairs at 2 instances. One is the bottom face of monopile with the adjacent soil surface and another one is the contact surface at the outer circumference of the monopile and the adjacent soil surface. The contact is set as finite sliding with "hard" contact in the normal behaviour and a friction penalty in the tangential behaviour with a friction coefficient of 0.33, and a maximum elastic slip tolerance of 0.005 for the circumference interface. Hard contact helps minimize the penetration of slave node surface to the master surface. The stiffer monopile surface is taken as the master surface and adjoining soil surface as the slave surface for the circumference interface. For bottom tie interface, the soil surface is taken as master surface and monopile as slave surface. This is done because of larger area of the soil surface element compared to the monopile bottom. The bottom interface has similar properties as the circumference interface, but "separation after contact" is disabled in order to make the interfaces tied. The interactions are shown in fig. 3.5.

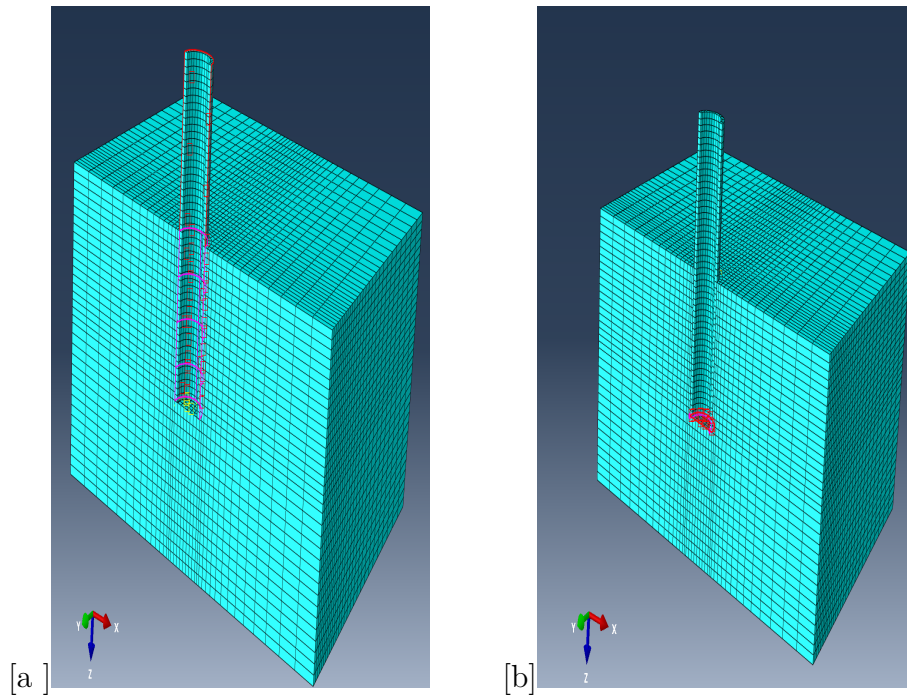


**Figure 3.5:** Interacting surfaces between soil and monopile

### 3.1.6 Step-definition

The finite element analysis is carried out in 4 subsequent steps after the initial setup. This provides a clearer visualisation of how different loads and steps act on the monopile as well as decreases a chance of convergence issues. A geostatic step is necessary to establish a geostatic equilibrium in the system. The initial geostatic stress field must be in equilibrium with the boundary condition, material properties and contact interface. This step also establishes the initial insitu stress conditions in the soil model. This step ensures the equilibrium conditions are met with the initial conditions and the boundary conditions set in the model. Geostatic stress and void ratio are defined at the initial setup itself, as predefined fields. The initial geostatic stress is taken as  $(\text{Total Mass Density} - \text{sp. weight of wetting liquid}) * \text{gravity} * \text{vertical depth}$ . It is calculated for both the soil layers and acts downwards.

Initial void ratio and pore pressure generated in the soil structure is also defined initially using a Void ratio and pore-pressure boundary condition.

In geostatic step, the self-weight and gravity acting on the assembly is also defined. In the next step, we define the tower load acting on the structure, through a static step. In the next static step, we apply the hydrodynamic load on the structure. The seismic loading is applied as a boundary condition in the final step as dynamic loading. Steps information is highlighted in table 3.4.

**Table 3.4:** Step Information

	Step Name	Procedure	Step time	Total time
1	Geostatic	STATIC,GENERAL	1.0	1.0
2	Towerload	STATIC,GENERAL	1.0	2.0
3	Windload	STATIC,GENERAL	2.0	4.0
4	Eqload	DYNAMIC	10.0	14.0

## 3.2 Loads used for the modelling process

As, illustrated in Chapter2, the structure is under constant and variable loads and moments, which need to be applied into the FEM model .

The wind turbine model used for the thesis is "NREL offshore 5-MW baseline wind turbine" [11], with the appropriate parameters as shown in fig. 3.6.

Rating	5 MW
Rotor Orientation, Configuration	Upwind, 3 Blades
Control	Variable Speed, Collective Pitch
Drivetrain	High Speed, Multiple-Stage Gearbox
Rotor, Hub Diameter	126 m, 3 m
Hub Height	90 m
Cut-In, Rated, Cut-Out Wind Speed	3 m/s, 11.4 m/s, 25 m/s
Cut-In, Rated Rotor Speed	6.9 rpm, 12.1 rpm
Rated Tip Speed	80 m/s
Overhang, Shaft Tilt, Precone	5 m, 5°, 2.5°
Rotor Mass	110,000 kg
Nacelle Mass	240,000 kg
Tower Mass	347,460 kg

**Figure 3.6:** NREL 5-MW Wind Turbine Specifications

### 3.2.1 Induced loads

The constant loads acting on the wind turbine is the weight of the the whole turbine ( excluding the monopile base weight) , which includes the rotor, nacelle and the tower mass. The constant loads are considered as a distributed load acting on the top face of the cylinder . The overall weight acting on the top face =

$$M_{rotor} + M_{nacelle} + M_{tower} = 110000 + 240000 + 347460 = 697460Kg$$

The self weight of the monopile is considered as gravity weight acting downwards.Also, as the whole structure is modelled in half profile due to symmetry, half of the weight i.e. 348730 kg.



### 3.2.2 Environmental loads

#### Hydrodynamic loads

Hydrodynamic loads in acting on the surface of the structure is calculated using Morisson's equation. Morisson equation provides simplicity in the variables as well as provides fairly accurate assesement of both the inertial and drag forces acting along the lateral faces of the cylindrical structure.

The mass coefficient  $C_m$  and drag coefficient  $C_d$  are taken as 2 and 0.7 respectively and the wave period is taken as  $T_w=9.87$  sec. Both the inertia force and drag force are taken into equation. Force acting on the cylindrical surface is given by :

$$F = \int_{-d}^{\varepsilon_0 \sin \omega t} \left\{ \frac{\pi D^2}{4} \rho C_M (\varepsilon_0 \text{ kg}/\omega) e^{kz} \cos(\omega t) + \frac{\rho}{2} C_D D (\varepsilon_0 \text{ kg}/\omega)^2 e^{2kz} \sin(\omega t) |\sin(\omega t)| \right\} dz \quad (3.2)$$

Wave height at  $H=2, 5, 10$  and  $15$  m respectively is calculated and the maximum values are applied to the finite model as surface forces through interpolation. The maximum data values are shown in the fig 3.7.

The hydrodynamic load is set as acting in horizontal direction at the top of the monopile face.

#### Seismic Loads

Seismic loads acting on the monopile is designed to address the ground motion activities effecting the structure. Seismic load is considered to be acting on the horizontal direction on the base layer (bedrock) of the soil model. The soil site is considered to be in the foot-wall of the rupture plane and is considered to be at a distance of  $50$  km from the surface projection of rupture. The nature of fault is considered as a normal fault. The time frequency for seismic loading is taken as  $10$  sec and no-after shock effects are considered. A  $5\%$  damping factor is applied for all magnitudes.

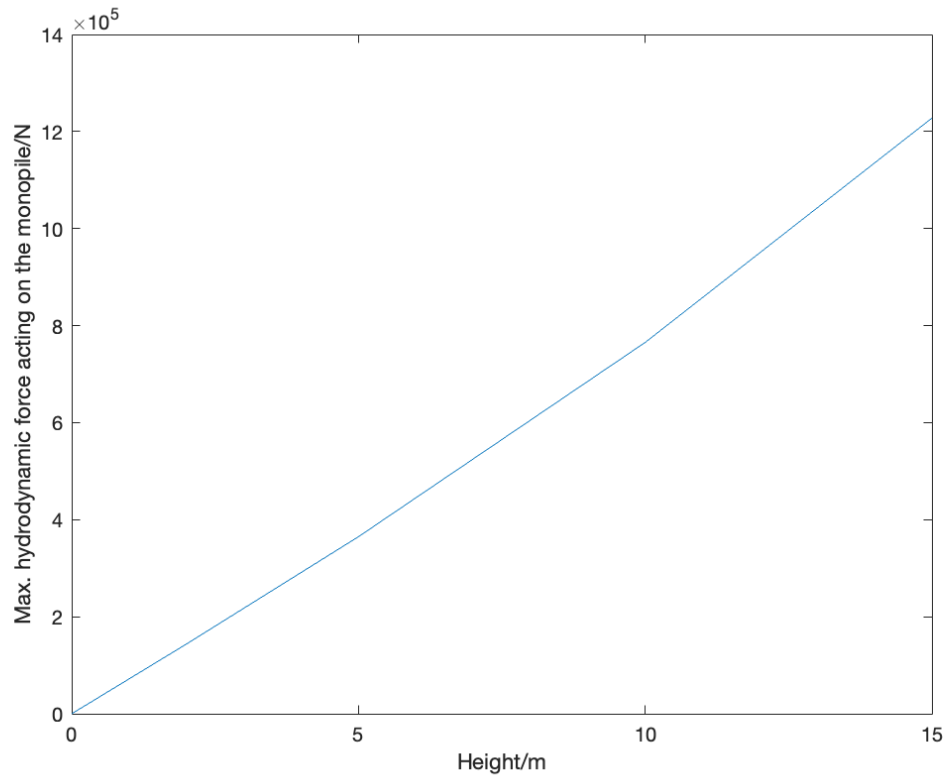


**Figure 3.7:** Maximum force at height 2, 5, 10 and 15m

### 3.3 Test Models

There are 3 cases of seismic loads that have been generated and used for simulation in the model. The median time-acceleration values are generated through ground motion model compiled by Chiou and Young , based on PEER NGA empirical database [5]. The model is governed through spectrum data of real earthquakes, used as a flat file to generate a suitable response spectrum depending upon the input parameters we use. Use of GMPE data instead of real earthquake data is used in order to keep all other seismic parameters intact and only change the seismic Magnitude Moments for all the cases. The input parameters for generation of PSA are defined in table 3.5 below and are calculated based on equations from the previous chapters:

For a comparative analysis, 4 test models are selected from the same soil-structure model, by varying the magnitude of seismic load in each case. All other soil and structure properties are kept intact including the boundary conditions and constraints. For the first test model, no seismic load is considered to study the

**Table 3.5:** Input parameters for NGAW-2 flatfiles

Parameters	Case 2	Case 3	Case 4
$\delta$	50°	50°	50°
$R_{JB}$ (km)	50	50	50
$R_X$ (km)	-38.7	-38.7	-38.7
W (km)	4.07	9.12	20.41
$Z_{TOR}$	8.36	5.84	0.455
$Z_{HYP}$	10.24	10.04	9.84
$\alpha$	-50°	-50°	-50°

deflection and stress development only through structure and wave loading, as shown in fig. 3.6.

**Table 3.6:** Test models and their corresponding seismic magnitude

Test no.	Magnitude Parameter
Case 1	-
Case 2	5 ( $M_L$ )
Case 3	6 ( $M_L$ )
Case 4	7 ( $M_L$ )

# Chapter 4

## Results and Analysis

### 4.1 Experimental results

In this section, the most relevant results from the simulation are highlighted on all the cases.

#### 4.1.1 Case 1

In case 1, no seismic forces are considered. The stress generation and any deflection that occurs is due to the geostatic stress generation and vertical loads acting on the monopile. Von Mises Stress is a good indicator of strength of a structure. Value of maximum Von Mises Stress, greater than the yield stress will lead to a structural failure. From fig. 4.1, it is evident that maximum stress in the model is generated in the mud level of monopile base. This correlates to similar parametric FEM analysis done by [19] on offshore support structures. A maximum value of deflection occurs at the monopile top of 0.04m and a deflection of 0.008m at the mud level of the monopile as shown in fig. 4.2.

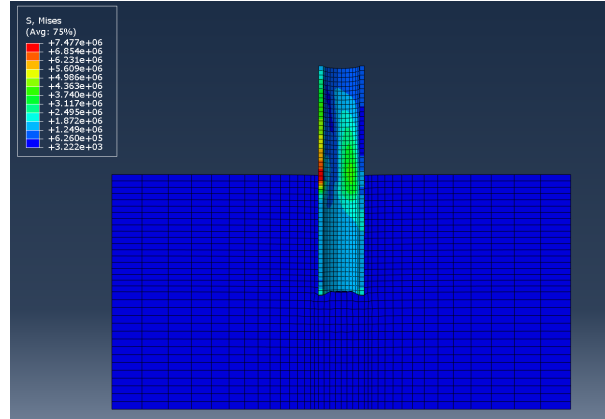


**Figure 4.1:** Von Mises Stress generation with no seismic load

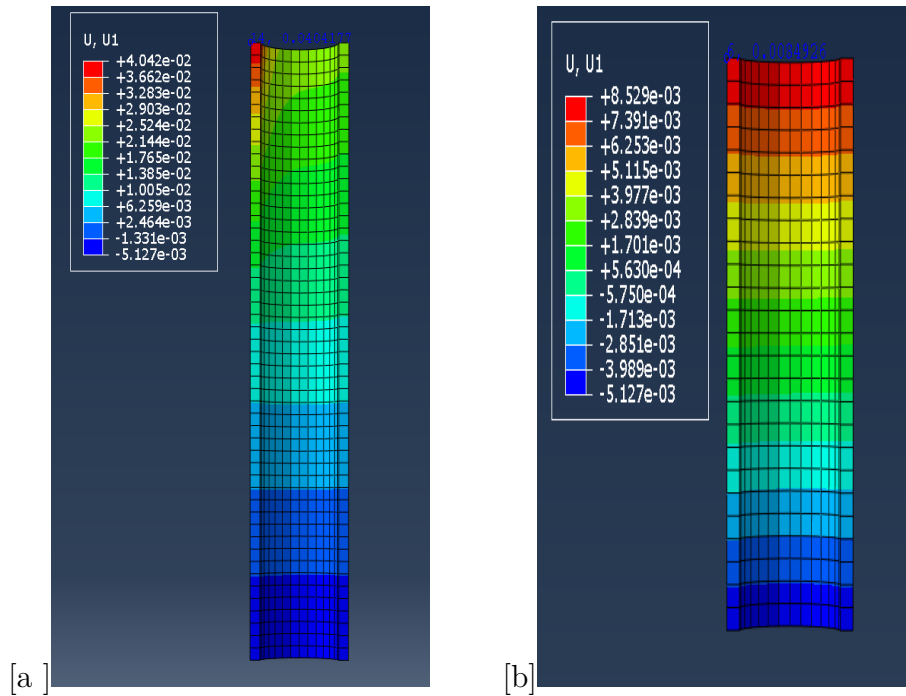


**Figure 4.2:** Deflection values on the monopile with no seismic load

#### 4.1.2 Case 2

As a continuation of case1, a seismic load is applied to the bottom layer of the soil model with a magnitude of 5 Magnitude Moment. The stress developed in the structure is 4.47 MPa around the edge of the monopile (see 4.4) and the maximum stress generated was 12 MPa as seen in fig. 4.5. Maximum deflection occurs in the monopile top face, which is evident due to the vertical tower load and horizontal wind load acting simultaneously and the maximum value of lateral displacement of

pile at mudline was observed as 0.75m (fig. ??). Significant deflection at the pile toe is also seen, which can be contributed to the soil stress acting on the monopile during initial steps.

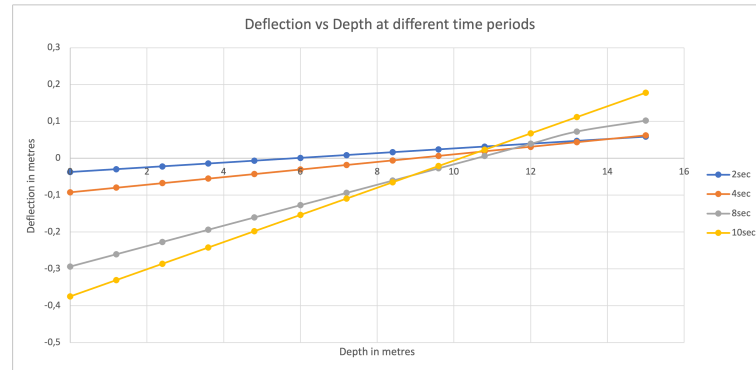


**Figure 4.3:** Deflection along the mudpile depth case 2

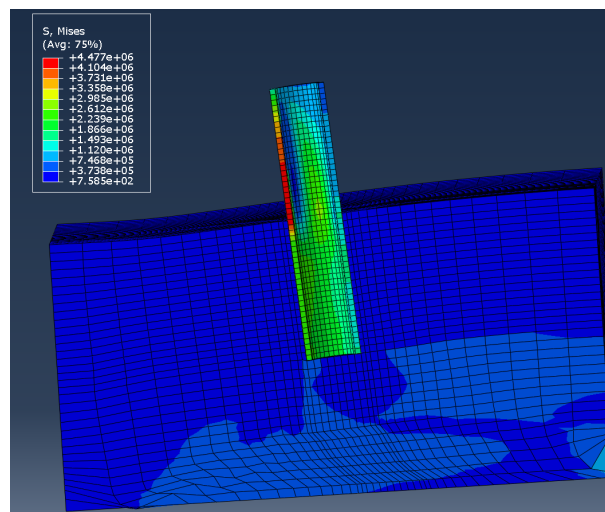


**Figure 4.4:** Von Mises Stress at the end of simulation case 2

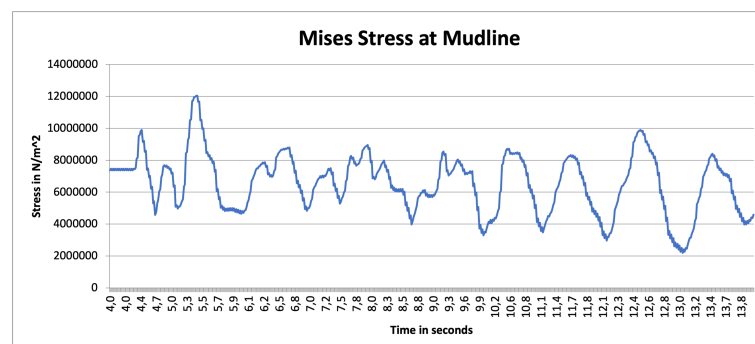


**Figure 4.5:** Von Mises Stress in the monopile at mud level case 2

Mudline rotation is calculated along a single node on monopile at mud-level through Abaqus query tool (see Appendices) . Maximum rotation angle was found to be  $0.02^\circ$ .

### 4.1.3 Case 3

A larger amplitude seismic load of 6 Magnitude is applied in this case. Higher deformation around the soil layers as well as larger deflection is monitored. Von Mises Stress developed in the pile node at mudlevel was 4.5 MPa 4.11 at the end of the analysis and the maximum value was obtained as 9.8 MPa as shown in 4.7 . The deflection along lateral direction of the monopile was 0.61m (see fig.4.8 )

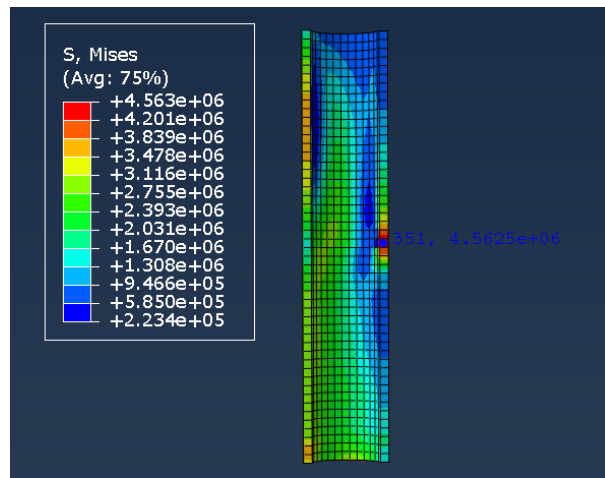


**Figure 4.6:** Von Mises Stress at the end of simulation case 3

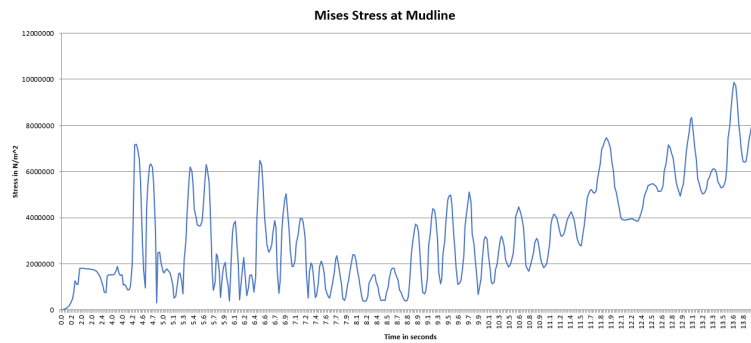


**Figure 4.7:** Von Mises Stress in the monopile at mud level case 3

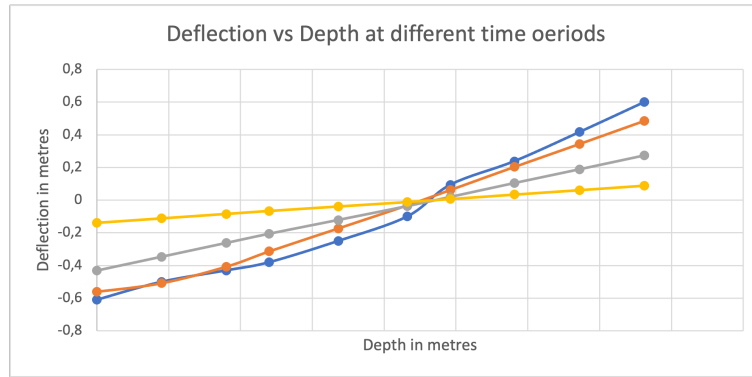


**Figure 4.8:** Deflection along the mudpile depth case 3

Mudline rotation along a single node was found as  $0.043^\circ$ .

#### 4.1.4 Case 4

Seismic load of magnitude 7 is applied in this case. Max. Von Mises Stress was generated on the monopile edge near the mud level, similar to other cases, with a value of 16.5 MPa (see fig. 4.10) and a value of 9.1 MPa at the end of simulation. Large deflections occur both at the mudline and the toe of the monopile upto 0.91m as in fig. 4.9.

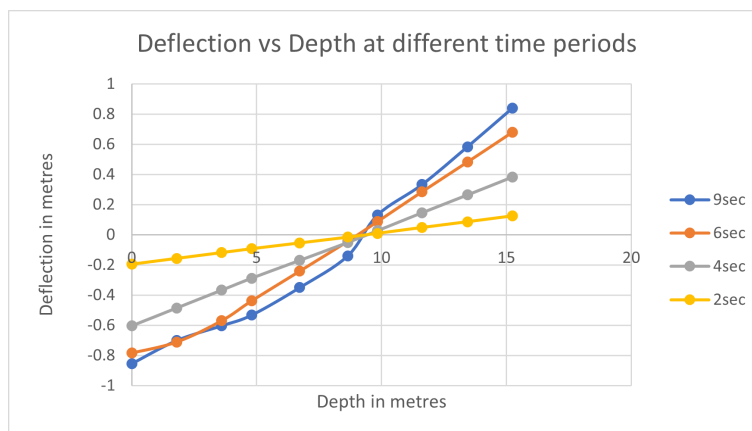


**Figure 4.9:** Deflection along the mudpile depth case 4



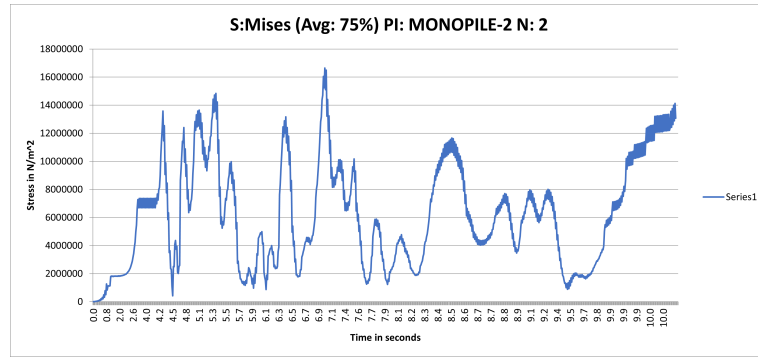


**Figure 4.10:** Von Mises Stress in the monopile at mud level case 4

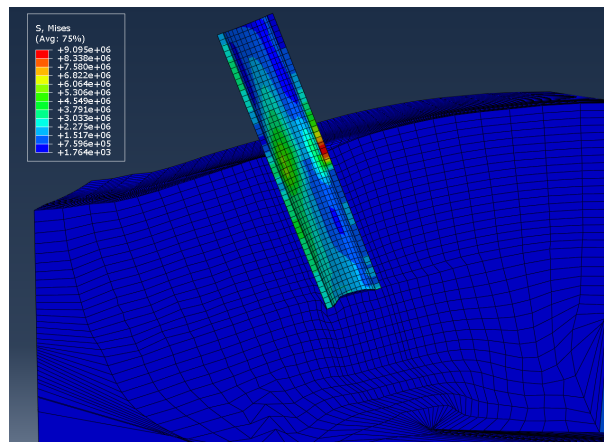


**Figure 4.11:** Von Mises Stress at the end of simulation case 4

Excessive mudline rotation around pile node was observed as  $1.18^\circ$ .

## 4.2 Analysis

The stress generated and lateral deflection occurring in all the cases was observed. In all the cases the stress on the pile is seen to be well below the ultimate yield strength of the material. It signifies that the material properties and the design criteria for the monopile model is sufficient to withstand drastic environmental conditions and loading without sustaining permanent deformation. Also, it is supported by the fact that angle of rotation of the monopile is much smaller than the threshold requirement of  $0.2^\circ$  in cases with magnitude 5 and 6. However, all the 3 cases (excluding case 1 with no seismic load) undergoes high lateral deflection, not only in the pile level at seabed, but also at the pile toe. This can be contributed to

the liquefaction of the soil, especially the upper layer of sandy soil, which results in larger deflection of monopile at higher loading conditions. This is also the reason for relatively lower values of Mises Stress generation in the monopile, as the liquefied soil can not transfer any sheer stress generation in the model. Similar results are observed by [8], where the monopile and caisson both undergo significant deflection under liquefiable soil. Higher rotation angle in case 4 can also be explained by this phenomenon. As, there is higher deflection at both the pile and soil model. This fact is more supported by the fact that all magnitude moments are applied from the same  $R_x$  distance, causing much higher amplitude waves at higher magnitude.

## Chapter 5

# Conclusion and Recommendations

In this chapter, conclusions regarding the findings and further recommendations have been discussed.

Effect of seismic loading needs careful study especially in case of monopiles with lower soil embedment. Analysis using a generic scenario, has shown the failure at ground level for higher magnitudes of earthquake. Stress response of monopiles even during higher seismic loading was satisfactory to prevent failure/deformation. Hence, material properties of monopile with S355 steel, as well as the overall dimensions of the monopile model can be deemed sufficient. Extensive research regarding ultimate strength of soil elements surrounding the pile is required instead, especially for saturated loose soil, as it was seen, the failure and liquefaction of soil layers can occur before the failure point in the monopile is reached. The effect of accurate soil modelling is highly influential upon the analysis results. Similar parameters of boundary conditions and loadings have differing values of displacement and stress, when comparing between the thesis results and the studies done beforehand. Further studies on Serviceability Limit State during seismic load is required for analysis during operation times.

# List of Figures

2.1	FEM Monopile model and monopile model with a transition piece [18]	6
2.2	Mohr-Coulumb failure criteria and Mohr's Circle	8
2.3	Major fault types during an earthquake (source:ucmp.berkeley.edu)	10
2.4	Wave propagation of seismic waves	12
2.5	Illustrations of GMPE parameters (source: NGAW2 database)	14
3.1	Process diagram for ABAQUS simulation	18
3.2	Front and isometric view of different soil layers	19
3.3	Meshed Structure of soil-monopile assembly	20
3.4	Boundary conditions applied on the model	21
3.5	Interacting surfaces between soil and monopile	22
3.6	NREL 5-MW Wind Turbine Specifications	24
3.7	Maximum force at height 2, 5, 10 and 15m	26
4.1	Von Mises Stress generation with no seismic load	29
4.2	Deflection values on the monopile with no seismic load	29
4.3	Deflection along the mudpile depth case 2	30
4.4	Von Mises Stress at the end of simulation case 2	30
4.5	Von Mises Stress in the monopile at mud level case 2	30
4.6	Von Mises Stress at the end of simulation case 3	31
4.7	Von Mises Stress in the monopile at mud level case 3	31
4.8	Deflection along the mudpile depth case 3	32
4.9	Deflection along the mudpile depth case 4	32
4.10	Von Mises Stress in the monopile at mud level case 4	33
4.11	Von Mises Stress at the end of simulation case 4	33
A.1	Response Spectrum of Magnitude 5	38
A.2	Response Spectrum of Magnitude 6	39
A.3	Response Spectrum of Magnitude 7	40
A.4	Rotation around mudlevel Case 2	41
A.5	Rotation around mudlevel Case 3	41
A.6	Rotation around mudlevel Case 4	42

# List of Tables

2.1	Foundation and Water depth . . . . .	5
2.2	Stability criterias . . . . .	16
3.1	Soil layer and their corresponding properties . . . . .	19
3.2	Mohr-Coulomb Model properties . . . . .	19
3.3	Elements and Nodes in the model . . . . .	20
3.4	Step Information . . . . .	23
3.5	Input parameters for NGAW-2 flatfiles . . . . .	27
3.6	Test models and their corresponding seismic magnitude . . . . .	27

# Appendix A

## Appendix

### A.1 PSA vs Time graph for all Moment magnitudes

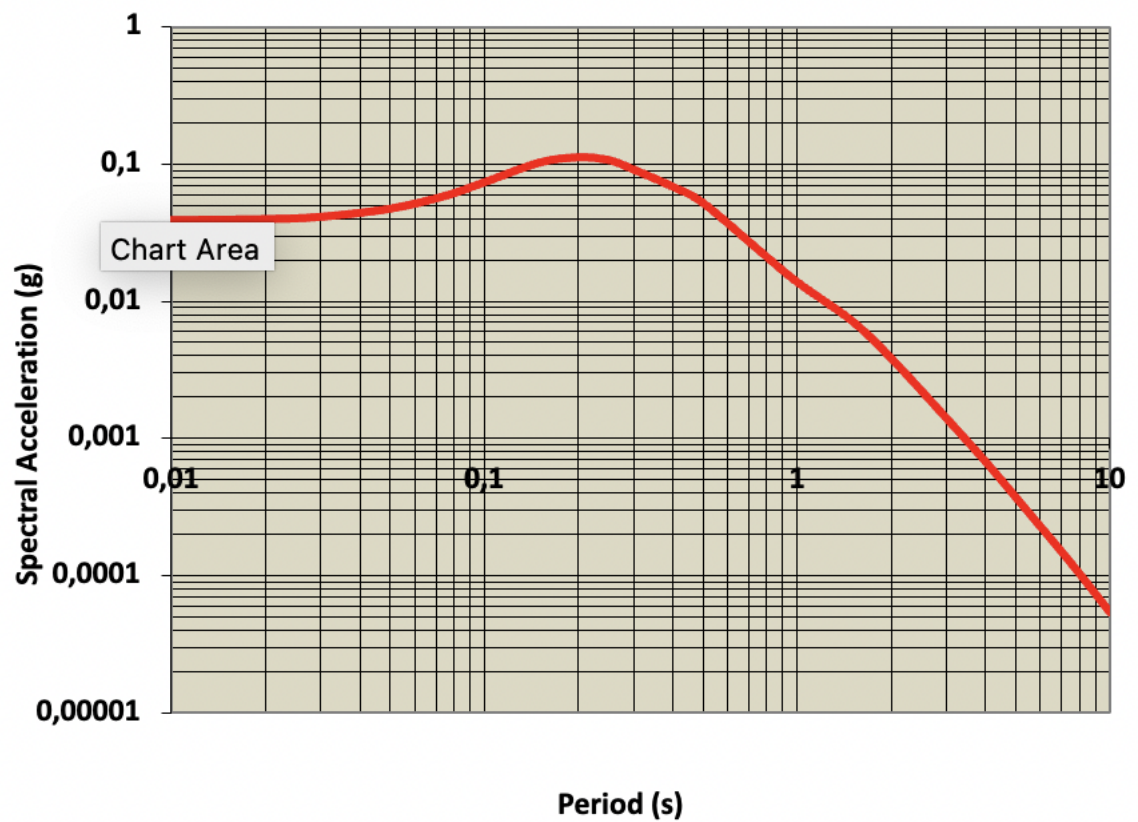
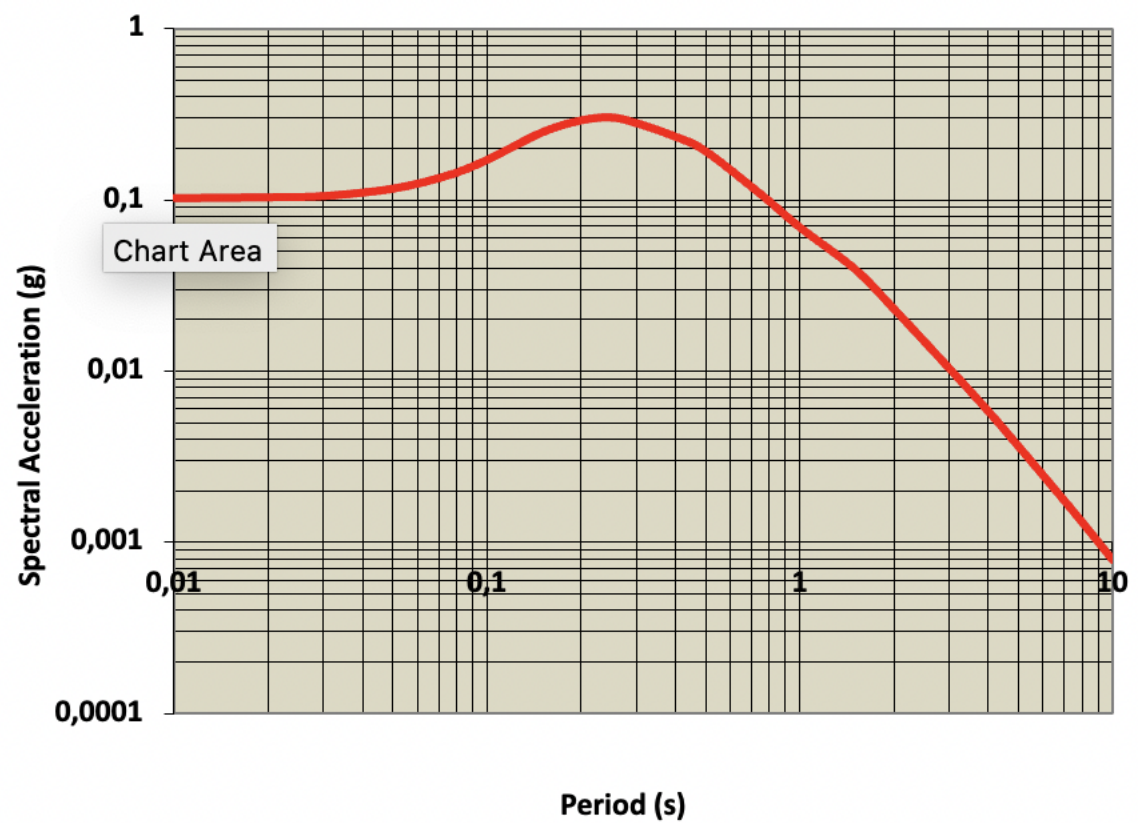
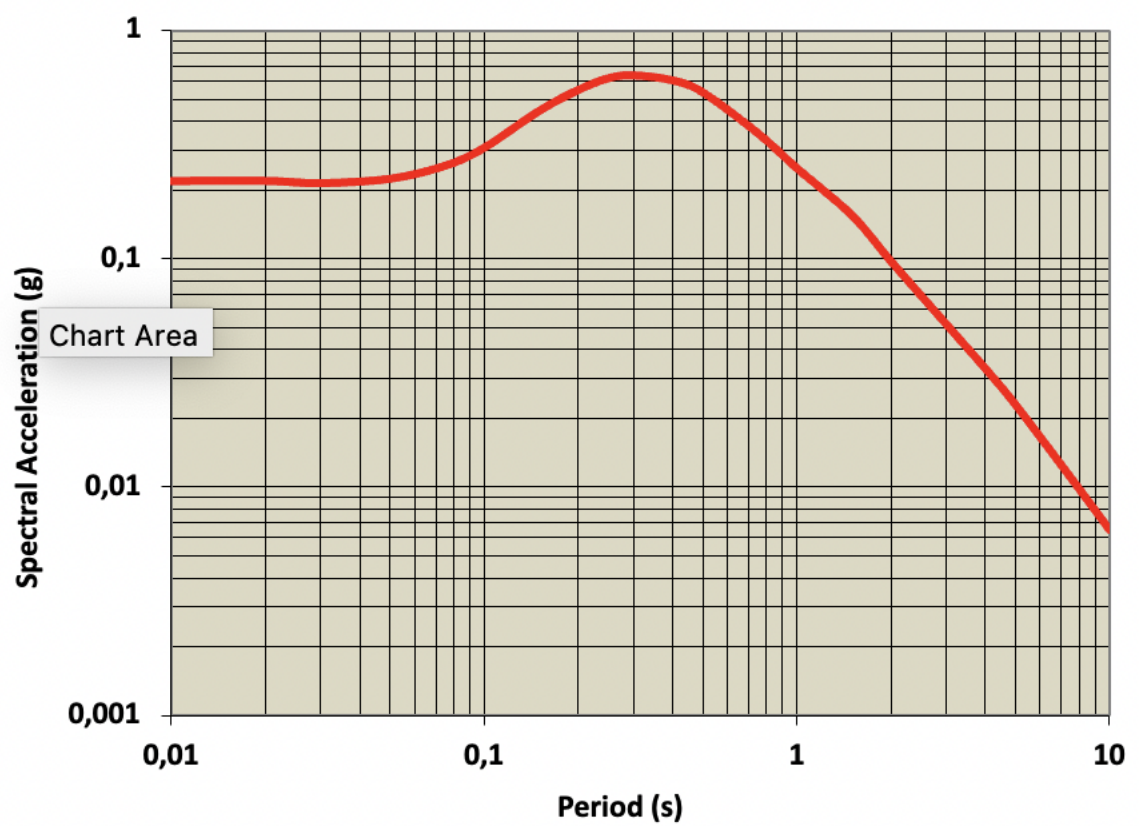


Figure A.1: Response Spectrum of Magnitude 5



**Figure A.2:** Response Spectrum of Magnitude 6



**Figure A.3:** Response Spectrum of Magnitude 7



## A.2 Rotation at pile node

Node: MONOPILE-2.126

	1	2	3	Magnitude
Base coordinates:	1.29000e+002,	4.00000e+001,	7.56000e+001,	-
Scale:	1.00000e+000,	1.00000e+000,	1.00000e+000,	-
Deformed coordinates (unscaled):	1.28311e+002,	4.00000e+001,	7.57914e+001,	-
Deformed coordinates (scaled):	1.28311e+002,	4.00000e+001,	7.57914e+001,	-
Displacement (unscaled):	-6.88929e-001,	1.74252e-032,	1.91365e-001,	7.15013e-001

Nodes for angle: MONOPILE-2.2, MONOPILE-2.6, MONOPILE-2.126

Angle in base coords: 9.00000e+001 degrees

Angle in deformed coords (unscaled): 8.99984e+001 degrees.

Angle in deformed coords (scaled): 8.99984e+001 degrees.

**Figure A.4:** Rotation around mudlevel Case 2

Nodes for angle: MONOPILE-2.126, MONOPILE-2.6, MONOPILE-2.2				
Angle in base coords: 9.00000e+001 degrees.				
Angle in deformed coords (unscaled): 9.00008e+001 degrees.				
Angle in deformed coords (scaled): 9.00008e+001 degrees.				
Node: MONOPILE-2.1				
	1	2	3	Magnitude
Base coordinates:	1.34400e+002,	4.00000e+001,	7.50000e+001,	-
Scale:	1.00000e+000,	1.00000e+000,	1.00000e+000,	-
Deformed coordinates (unscaled):	1.31739e+002,	4.00000e+001,	7.43199e+001,	-
Deformed coordinates (scaled):	1.31739e+002,	4.00000e+001,	7.43199e+001,	-
Displacement (unscaled):	-2.66082e+000,	6.12834e-032,	-6.80109e-001,	2.74636e+000
Node: MONOPILE-2.10				
	1	2	3	Magnitude
Base coordinates:	1.35000e+002,	4.00000e+001,	7.50000e+001,	-
Scale:	1.00000e+000,	1.00000e+000,	1.00000e+000,	-
Deformed coordinates (unscaled):	1.32315e+002,	4.00000e+001,	7.41504e+001,	-
Deformed coordinates (scaled):	1.32315e+002,	4.00000e+001,	7.41504e+001,	-
Displacement (unscaled):	-2.68524e+000,	5.98486e-032,	-8.49578e-001,	2.81643e+000
Node: MONOPILE-2.139				
	1	2	3	Magnitude
Base coordinates:	1.35000e+002,	4.00000e+001,	7.56000e+001,	-
Scale:	1.00000e+000,	1.00000e+000,	1.00000e+000,	-
Deformed coordinates (unscaled):	1.32484e+002,	4.00000e+001,	7.47260e+001,	-
Deformed coordinates (scaled):	1.32484e+002,	4.00000e+001,	7.47260e+001,	-
Displacement (unscaled):	-2.51581e+000,	1.39505e-032,	-8.73972e-001,	2.66329e+000
Nodes for angle: MONOPILE-2.1, MONOPILE-2.10, MONOPILE-2.139				
Angle in base coords: 9.00000e+001 degrees.				
Angle in deformed coords (unscaled): 8.99957e+001 degrees.				
Angle in deformed coords (scaled): 8.99957e+001 degrees.				

**Figure A.5:** Rotation around mudlevel Case 3

```

Node: MONOPILE-2.279
      1          2          3      Magnitude
Base coordinates:  1.29000e+002,  4.00000e+001,  7.26000e+001,  -
Scale:            1.00000e+000,  1.00000e+000,  1.00000e+000,  -
Deformed coordinates (unscaled):  1.25173e+002,  3.99995e+001,  7.44692e+001,  -
Deformed coordinates (scaled):    1.25173e+002,  3.99995e+001,  7.44692e+001,  -
Displacement (unscaled):  -3.82681e+000,  -4.60709e-004,  1.86918e+000,  4.25891e+000

Node: Soil foundation-2.90
      1          2          3      Magnitude
Base coordinates:  1.29000e+002,  4.00000e+001,  7.50000e+001,  -
Scale:            1.00000e+000,  1.00000e+000,  1.00000e+000,  -
Deformed coordinates (unscaled):  1.25356e+002,  4.00000e+001,  7.49202e+001,  -
Deformed coordinates (scaled):    1.25356e+002,  4.00000e+001,  7.49202e+001,  -
Displacement (unscaled):  -3.64446e+000,  -4.37666e-034,  -7.98122e-002,  3.64534e+000

Node: Soil foundation-2.1712
      1          2          3      Magnitude
Base coordinates:  1.29075e+002,  3.93324e+001,  7.50000e+001,  -
Scale:            1.00000e+000,  1.00000e+000,  1.00000e+000,  -
Deformed coordinates (unscaled):  1.25434e+002,  3.93324e+001,  7.49126e+001,  -
Deformed coordinates (scaled):    1.25434e+002,  3.93324e+001,  7.49126e+001,  -
Displacement (unscaled):  -3.64166e+000,  -1.13390e-033,  -8.74094e-002,  3.64271e+000

Nodes for angle: MONOPILE-2.279, Soil foundation-2.90, Soil foundation-2.1712
Angle in base coords:  9.00000e+001 degrees.
Angle in deformed coords (unscaled):  9.18384e+001 degrees.
Angle in deformed coords (scaled):  9.18384e+001 degrees.

```

Figure A.6: Rotation around mudlevel Case 4

# Bibliography

- [1] AAMODT, K. K. Soil reaction curves and damping for monopile design in clay. *Marine Structures* 65 (2019), 94–113. <https://ntnuopen.ntnu.no/ntnu-xmlui/handle/11250/2625271>.
- [2] ARANY, L., BHATTACHARYA, S., MACDONALD, J. H., AND HOGAN, S. J. *A Critical Review of Serviceability Limit State Requirements for Monopile Foundations of Offshore Wind Turbines*. Offshore Technology Conference. May 2015. <https://doi.org/10.4043/25874-MS>.
- [3] ATHANASOPOULOS, G., PELEKIS, P., AND ANAGNOSTOPOULOS, G. Effect of soil stiffness in the attenuation of Rayleigh-wave motions from field measurements. *Soil Dynamics and Earthquake Engineering* 19 (June 2000), 277–288.
- [4] BULJAC, A., KOZMAR, H., YANG, W., AND KAREEM, A. Concurrent wind, wave and current loads on a monopile-supported offshore wind turbine. *Engineering Structures* 255 (Mar. 2022), 113950. <https://www.sciencedirect.com/science/article/pii/S0141029622001067>.
- [5] CHIOU, B.-J., AND YOUNGS, R. R. An NGA Model for the Average Horizontal Component of Peak Ground Motion and Response Spectra. *Earthquake Spectra* 24, 1 (Feb. 2008), 173–215. <https://doi.org/10.1193/1.2894832>.
- [6] DAVENNE, L., RAGUENEAU, F., MAZARS, J., AND IBRAHIMBEGOVIC, A. Efficient approaches to finite element analysis in earthquake engineering. *Computers & Structures* 81 (May 2003), 1223–1239.
- [7] DE RISI, R., BHATTACHARYA, S., AND GODA, K. Seismic performance assessment of monopile-supported offshore wind turbines using unscaled natural earthquake records. *Soil Dynamics and Earthquake Engineering* 109 (June

- 2018), 154–172. <https://www.sciencedirect.com/science/article/pii/S0267726117309454>.
- [8] ESFEH, P. K., AND KAYNIA, A. M. Earthquake response of monopiles and caissons for Offshore Wind Turbines founded in liquefiable soil. *Soil Dynamics and Earthquake Engineering* 136 (Sept. 2020), 106213. <https://www.sciencedirect.com/science/article/pii/S0267726120300646>.
- [9] HELWANY, S. *Applied Soil Mechanics with ABAQUS Applications*, 1st edition ed. Wiley, 2007. [https://www.academia.edu/39417794/APPLIED\\_SOIL\\_MECHANICS\\_with\\_ABAQUS\\_Applications](https://www.academia.edu/39417794/APPLIED_SOIL_MECHANICS_with_ABAQUS_Applications).
- [10] HORWATH, S., HASSRICK, J., GRISMALA, R., AND DILLER, E. Comparison of Environmental Effects from Different Offshore Wind Turbine Foundations. Tech. Rep. OCS Study BOEM 2021-053, U.S. Dept. of the Interior, Bureau of Ocean Energy Management, 2021.
- [11] JONKMAN, J., BUTTERFIELD, S., MUSIAL, W., AND SCOTT, G. Definition of a 5-MW Reference Wind Turbine for Offshore System Development. Tech. Rep. NREL/TP-500-38060, 947422, Feb. 2009. <http://www.osti.gov/servlets/purl/947422-nhrlni/>.
- [12] JUHARI, N. Recommended Practice for Planning, Designing and Constructing Fixed Offshore Platforms—Working Stress Design API recommended Practice 2A-WSD (RP 2A-WSD). Tech. rep., American Petroleum Institute, 2000. [https://www.academia.edu/37079635/Recommended\\_Practice\\_for\\_Planning\\_Designing\\_and\\_Constructing\\_Fixed\\_Offshore\\_Platforms\\_Working\\_Stress\\_Design\\_API\\_RECOMMENDED\\_PRACTICE\\_2A\\_WSD\\_RP\\_2A\\_WSD\\_TWENTY\\_FIRST\\_EDITION\\_DECEMBER\\_2000](https://www.academia.edu/37079635/Recommended_Practice_for_Planning_Designing_and_Constructing_Fixed_Offshore_Platforms_Working_Stress_Design_API_RECOMMENDED_PRACTICE_2A_WSD_RP_2A_WSD_TWENTY_FIRST_EDITION_DECEMBER_2000).
- [13] KAKLAMANOS, J., BAISE, L. G., AND BOORE, D. M. Estimating Unknown Input Parameters when Implementing the NGA Ground-Motion Prediction Equations in Engineering Practice. *Earthquake Spectra* 27, 4 (Nov. 2011), 1219–1235. <https://doi.org/10.1193/1.3650372>.
- [14] KATSANOS, E. I., THÖNS, S., AND GEORGAKIS, C. T. Wind turbines and seismic hazard: A state-of-the-art review. *Wind Energy* 19, 11 (2016), 2113–2133. <https://onlinelibrary.wiley.com/doi/abs/10.1002/we.1968>.

- [15] KAYNIA, A. M. Seismic considerations in design of offshore wind turbines. *Soil Dynamics and Earthquake Engineering* 124 (Sept. 2019), 399–407. <https://linkinghub.elsevier.com/retrieve/pii/S0267726117309363>.
- [16] MALHOTRA, S. Selection, Design and Construction of Offshore Wind Turbine Foundations. In *Wind Turbines*. Al-Bahadly, Ibrahim, Apr. 2011.
- [17] MUSIAL, W., SPITSEN, P., BEITER, P., DUFFY, P., MARQUIS, M., COOPERMAN, A., HAMMOND, R., AND SHIELDS, M. Offshore Wind Market Report: 2021 Edition. 119.
- [18] RAKTATE, T., AND CHOUDHARY, R. Design of Monopile Foundation for Offshore Wind Turbine. *E3S Web Conf.* 170 (2020), 01024. <https://www.e3s-conferences.org/10.1051/e3sconf/202017001024>.
- [19] SAINZ DE LA MAZA GARRASTATXU, M. *Parametric Modellig and Fatigue Damage Assessment of Offshore Wind Turbine Support Structures*. PhD thesis, Universidad del País Vasco, Dec. 2016. <https://addi.ehu.es/handle/10810/19944>.
- [20] VELARDE, J. Design of Monopile Foundations to Support the DTU 10 MW Offshore Wind Turbine. Master’s thesis, Delft University of Science and Technology, 2015. <https://repository.tudelft.nl/islandora/object/uuid%3Aed2c91db-450e-4d64-86a5-9e410bd0ecda>.
- [21] XU, R. Stress analysis of a monopile foundation under the hammering loads. Master’s thesis, Norwegian University of Science and Technology, 2017. <https://ntnuopen.ntnu.no/ntnu-xmlui/handle/11250/2452272>.